

Some novel features of the Non-Universal Higgs Model

Leszek Roszkowski

*Department of Physics and Astronomy, University of Sheffield,
Sheffield S3 7RH, England E-mail: L.Roszkowski@sheffield.ac.uk*

Roberto Ruiz de Austri

*Instituto de Física Corpuscular, IFIC-UV/CSIC,
Valencia, Spain
E-mail: rruiz@ific.uv.es*

Roberto Trotta

*Astrophysics Group, Imperial College London
Blackett Laboratory, Prince Consort Road, London SW7 2AZ, UK E-mail:
r.trotta@imperial.ac.uk*

Yue-Lin Sming Tsai

*Department of Physics and Astronomy, University of Sheffield,
Sheffield S3 7RH, England E-mail: php06yt@sheffield.ac.uk*

Tom A. Varley

*Department of Physics and Astronomy, University of Sheffield,
Sheffield S3 7RH, England E-mail: php06tav@sheffield.ac.uk*

ABSTRACT: We examine the Non-Universal Higgs Model (NUHM) with the help of a Markov Chain Monte Carlo scanning technique and Bayesian statistics. The method allows us to reveal more fully the remarkably rich and complex structure of the model and also some new interesting features. In particular we find that, for large ranges of parameters, the neutralino dark matter in the model is higgsino-like with mass close to 1 TeV. This feature does depend to some extent on the prior but generically results from a mild focussing effect in the running of one of the Higgs masses that we also point out. On the other hand, the usual bino-like neutralino is also present, and in some sense is favored by a more robust prior and a better average chi-square. In spite of experimental constraints often favoring different regions of parameter space than in the Constrained MSSM, most observational consequences appear fairly similar, which will make it challenging to experimentally distinguish the two models.

KEYWORDS: Supersymmetric Effective Theories, Cosmology of Theories beyond the SM, Dark Matter.

Contents

1. Introduction	1
2. Outline of the statistical treatment	3
3. Probability maps of NUHM parameters and observables	6
4. Collider signatures	16
5. Dark matter signatures	18
6. Conclusions	22

1. Introduction

Softly broken low-energy supersymmetry (SUSY) has many attractive features [1]. For example, unlike the Standard Model (SM), it provides an elegant solution to the gauge hierarchy problem and a natural weakly-interacting dark matter (DM) candidate, in addition to accounting for gauge coupling unification. On the other hand, SUSY itself has to be (softly) broken in order to make contact with reality, which in the general Minimal Supersymmetric Standard Model (MSSM) introduces a large number of new free parameters, namely the soft masses. Because of SUSY's natural link with grand unification theories (GUTs), one often explores SUSY models by imposing various boundary conditions at the GUT scale. The most popular model of this class is the Constrained MSSM (CMSSM) [2], in which not only do gaugino soft masses unify to $m_{1/2}$ but also soft masses of all the sfermions and Higgs doublets unify to m_0 . These parameters, along with a common trilinear mass parameter A_0 and the ratio of Higgs vacuum expectation values $\tan\beta$, form the four continuous parameters of the CMSSM. The relative simplicity of the model makes a very attractive playground for many studies.

On the other hand, precisely because of its economy, the CMSSM may be missing some features of unified models with less restrictive boundary conditions at the unification scale. In particular, the assumption of Higgs (soft) mass unification with those of the sfermions does not seem strongly motivated since the Higgs and matter fields belong to different supermultiplets. One explicit example where this is the case is a minimal $SO(10)$ supersymmetric model (MSO₁₀SM) [3], which is well motivated and opens up a qualitatively new region of parameter space [4]. Models like this provide a good motivation for exploring a wider class of phenomenological models in which the soft masses m_{H_u} and m_{H_d} (as defined

at the GUT scale) of the two Higgs doublets are treated as independent parameters and which come under the name of the Non-Universal Higgs Model (NUHM) [5].¹

In the NUHM, there are therefore six continuous free parameters:

$$m_0, m_{1/2}, \tan \beta, A_0, m_{H_u} \text{ and } m_{H_d}. \quad (1.1)$$

The Renormalization Group Equations (RGEs) are then used to evaluate masses and couplings at the electroweak scale and the Higgs potential is minimized in the usual way. Electroweak Symmetry Breaking (EWSB) conditions for NUHM read:

$$\mu^2 = \frac{m_{H_d}^2 - m_{H_u}^2 \tan^2 \beta}{\tan^2 \beta - 1} - \frac{1}{2} m_Z^2, \quad (1.2)$$

$$m_A^2 = m_{H_d}^2 + m_{H_u}^2 + 2\mu^2, \quad (1.3)$$

where m_A stands for the mass of the pseudoscalar Higgs A and μ is the SUSY-preserving Higgs/higgsino mass parameter. In the above equations all the parameters are evaluated at the usual electroweak scale $M_{\text{SUSY}} \equiv \sqrt{m_{\tilde{t}_1} m_{\tilde{t}_2}}$ (where $m_{\tilde{t}_1, \tilde{t}_2}$ denote the masses of the scalar partners of the top quark), chosen so as to minimize higher order loop corrections. At M_{SUSY} the (1-loop corrected) conditions of electroweak symmetry breaking (EWSB) are imposed and the SUSY spectrum is computed at m_Z .

Like in the CMSSM the sign of μ remains undetermined. On the other hand, unlike in the CMSSM, because of the larger number of free parameters, both μ and m_A can be treated as free parameters in place of high scale parameters m_{H_u} and m_{H_d} . This will have an important impact on the properties of the model. In particular, the ability to effectively choose the position of the A funnel or to tune μ for a given point in the parameter space to give a correct relic abundance of the neutralino DM will lead to very different phenomenological predictions, as we will see below.

The moderately increased number of free parameters of the NUHM has been shown to lead to a rich and distinct phenomenology (see for example [8, 9, 10, 11] and references therein). In particular, there is a larger variety of choices for the lightest superpartner (LSP). In the CMSSM the LSP is either the lightest neutralino or the lighter stau or, in some relatively rare case, the lighter stop. In contrast, in the NUHM, the LSP can in addition be a sneutrino or right handed selectron [9]. Assuming the LSP to be the dark matter in the Universe, eliminates states that are not electrically neutral and leads to a non-trivial constraint on the parameter space. However, the near degeneracy of many states with the LSP leads to a great variety of co-annihilation channels. Also, given that m_A can now be treated as effectively a free parameter, the resonance channel can be important in different ways from the CMSSM. Also, as we will see, in a large region of the parameter space the neutralino will actually be higgsino-like but giving the correct dark matter abundance. And although in general a lighter higgsino-dominated LSP underproduces dark matter [12], as its mass increases the transition to higgsino dark matter can provide an acceptable relic density. In general these effects can also conspire to give the correct relic density in different parts of the parameter space.

¹A reduced version of NUHM with $m_{H_u} = m_{H_d}$ has also been examined in several papers, eg [6, 7].

The larger number of parameters makes a full exploration of the NUHM parameter space even more challenging than that of the CMSSM. Additionally, varying relevant Standard Model parameters can lead to important consequences, which has been shown in recent studies of the CMSSM with the help of Markov Chain Monte Carlo (MCMC) scanning technique coupled to Bayesian statistics. There are distinct advantages in doing this, such as being able to efficiently explore the parameter space varying all inputs simultaneously and being able to incorporate errors, both theoretical and experimental, as well as relevant SM parameters correctly. This will allow us to efficiently explore regions of the model's parameters that were not easily accessible in the usual fixed-grid scans, while addressing, at the same time, questions about the dependence of the results on priors.

With this in mind in this paper we apply the same approach to investigate the NUHM. We employ the package **SuperBayeS** [13] and include all the relevant constraints coming from experiment to our scan. In particular, included are the branching ratio of $b \rightarrow s\gamma$, the difference $\delta(g-2)_\mu$ between the experimental and SM values of the magnetic moment of the muon, the LEP limits on sparticle and Higgs masses, the 5 year WMAP limits on the relic density $\Omega_{\text{CDM}}h^2$ and several other measured but imprecisely known quantities of the SM that SUSY can contribute to. A full list of constraints used and the exact numbers used in the analysis will be given below.

In this paper, we present several features of the NUHM which arose in light of our global MCMC scans. It should be noted that we take a wider range of parameters than previous scans in the literature (up to 4 TeV in the case of the soft masses), and the MCMC technique allows us to vary all our parameters such that we also consider $A_0 \neq 0$, while at the same time varying relevant SM parameters.

The paper is organised as follows. In sec. 2 we summarise the statistical formalism that we employ and list the constraints that we apply. Then, in sec. 3 we present the ranges of NUHM parameters that are favoured by two distinctively different prior choices and discuss their main features, including the possibility of higgsino DM and a mild focussing effect. Next, in sec. 4 we present some implications for phenomenology, including direct and indirect SUSY searches in colliders, while in sec. 5 we discuss prospects of direct and indirect detection of the neutralino dark matter in the model. We conclude and summarize our results in sec. 6.

2. Outline of the statistical treatment

In comparison to earlier analyses of the CMSSM [14, 15, 16] here we have a larger base parameter set, defined by

$$\theta = (m_{1/2}, m_0, A_0, \tan \beta, m_{H_u}, m_{H_d}), \quad (2.1)$$

where again we fix $\text{sgn}(\mu) = +1$. As the relevant SM parameters, when varied over their experimental ranges, have impact on the observable quantities, fixing them at their central values would lead to inaccurate results. Instead, here we incorporate them explicitly as free parameters (which are then constrained using their measured values), which we call

nuisance parameters ψ , where

$$\psi = (M_t, m_b(m_b)^{\overline{MS}}, \alpha_{em}(m_Z)^{\overline{MS}}, \alpha_s(m_Z)^{\overline{MS}}). \quad (2.2)$$

In eq. (2.2) M_t denotes the pole top quark mass, while the other three parameters: $m_b(m_b)^{\overline{MS}}$ – the bottom quark mass evaluated at m_b , $\alpha_{em}(M_Z)^{\overline{MS}}$ and $\alpha_s(M_Z)^{\overline{MS}}$ – respectively the electromagnetic and the strong coupling constants evaluated at the Z pole mass m_Z – are all computed in the \overline{MS} scheme. Using notation consistent with previous analyses we define our now ten *basis parameters* as

$$m = (\theta, \psi) \quad (2.3)$$

which we will be scanning simultaneously with the MCMC technique. For each choice of m various colliders or cosmological observables will be calculated. These derived variables are denoted by $\xi = (\xi_1, \xi_2, \dots)$, which are then compared with the relevant available data d . The quantity we are interested in is the *posterior probability density function* (or simply posterior) $p(m|d)$ which gives the probability of the parameters after the constraints coming from the data have been applied. The posterior follows from Bayes' theorem,

$$p(m|d) = \frac{p(d|\xi)\pi(m)}{p(d)}, \quad (2.4)$$

where $p(d|\xi)$, taken as a function of ξ for *fixed data* d , is called the *likelihood* (where the dependence of $\xi(m)$ is understood). The likelihood is the quantity that compares the data with the derived observables. $\pi(m)$ is the *prior* which encodes our state of knowledge of the parameters before comparison with the data. This state of knowledge is then updated by the likelihood to give us the posterior. $p(d)$ is called the *evidence* or *model likelihood*, and in our analysis can be treated as a normalisation and hence is ignored subsequently. (See instead [17] for an example of how the evidence can be used for model comparison purposes.)

As in previous papers, we have chosen the ranges of the base parameters as follows: $50 \text{ GeV} < m_0, m_{1/2} < 4 \text{ TeV}$, $|A_0| < 7 \text{ TeV}$ and $2 < \tan \beta < 62$. For the Higgs soft mass parameters we take $0 < m_{H_u}, m_{H_d} < 4 \text{ TeV}$. Notice that by this range of m_{H_u} and m_{H_d} , and taking $\text{sgn}(\mu) > 0$, we automatically satisfy the GUT stability constraint of ref. [9]. We scan through the above parameters assuming two different choices of priors:

- flat priors in all the NUHM parameters;
- log priors, that are flat in $\log m_{1/2}$, $\log m_0$, $\log m_{H_u}$ and $\log m_{H_d}$, while for A_0 and $\tan \beta$ we keep flat priors.

As before [19], our rationale for this choice of priors is that they are distinctively different. The reason why we apply different priors to soft mass parameters only is that they play a dominant rôle in the determination of the masses of the superpartners and Higgs bosons. As we shall show below, the choice of log priors is actually more suitable to the exploration of the parameter space for both physical and statistical reasons. From the

SM (nuisance) parameter	Mean value μ	Uncertainty σ (exper.)	ref.
M_t	172.6 GeV	1.4 GeV	[23]
$m_b(m_b)^{\overline{MS}}$	4.20 GeV	0.07 GeV	[24]
$\alpha_s(M_Z)^{\overline{MS}}$	0.1176	0.002	[24]
$1/\alpha_{\text{em}}(M_Z)^{\overline{MS}}$	127.955	0.018	[24]

Table 1: Experimental mean μ and standard deviation σ adopted for the likelihood function for SM (nuisance) parameters, assumed to be described by a Gaussian distribution.

physical point of view, log priors explore in much greater detail the low-mass region, which exhibits many fine-tuned points that can easily be missed by a flat prior scan. From the statistical point of view, log priors give the same *a priori* weight to all orders of magnitude in the masses, and thus appear to be less biased to giving larger statistical *a priori* weights to the large mass region, which under a flat prior has a much larger volume in parameter space, similar to the CMSSM case [19]. We will show below how this leads to a large “volume effect” in the posterior, which does not reflect the average quality of fit of those points. In fact, here the volume effect is expected to be even larger than in the CMSSM, due to the larger number of parameters. For these reasons, we regard the results obtained with the log prior as the more robust and we present flat prior cases mostly for comparison.

The SM parameters are assigned flat priors and are then constrained by applying Gaussian likelihoods representing the experimental observations (see table 1). The issue of priors is irrelevant for SM parameters, as they are directly constrained by observation. The predictions for the observable quantities are obtained by using SoftSusy 2.0.5 and DarkSusy 4.0 [20, 21] as implemented in the **SuperBayeS** code. The likelihoods for the relevant observables are taken as Gaussian (for measured observables) with mean μ , experimental errors σ and theoretical errors τ (see the detailed explanation in [15]). In the case where there only an experimental limit is available, this is given, along with the theoretical error. The smearing out of bounds and combination of experimental and theoretical errors is handled in an identical manner to [15].

As ever, any points that fail to provide radiative EWSB, give us tachyonic sleptons or provide the LSP which is not the lightest neutralino are excluded. As in previous works [15, 16, 18], we adopt a Metropolis-Hastings MCMC algorithm to sample the parameter space. We have also cross-checked our results by employing the more recently implemented MultiNest algorithm [22, 19] and the findings are compatible (up to numerical noise). The results presented in the rest of this paper are obtained from the 25 chains that were used, garnering a total of 3×10^5 samples each, with an acceptance rate of around 4%. Convergence criteria are the same as in our previous papers [15, 16, 18].

Although in this paper the profile likelihood is not used (see instead [19] for a detailed analysis), some best fit points will be shown in the 2D posterior plots for comparison. This is useful to identify volume effects arising from the prior, namely situations where the density of posterior samples (and hence, the corresponding posterior probability density) is large due to a large volume of parameter space and not because of large likelihood.

Observable	Mean value	Uncertainties		ref.
	μ	σ (exper.)	τ (theor.)	
m_W	80.392 GeV	29 MeV	15 MeV	[25]
$\sin^2 \theta_{\text{eff}}$	0.23153	16×10^{-5}	15×10^{-5}	[25]
$\delta(g-2)_\mu \times 10^{10}$	27.5	8.4	1	[26]
$BR(\overline{B} \rightarrow X_s \gamma) \times 10^4$	3.55	0.26	0.21	[27]
ΔM_{B_s}	17.33 ps $^{-1}$	0.12 ps $^{-1}$	4.8 ps $^{-1}$	[28]
$BR(\overline{B}_u \rightarrow \tau \nu) \times 10^4$	1.32	0.49	0.38	[27]
$\Omega_\chi h^2$	0.1099	0.0062	$0.1 \Omega_\chi h^2$	[29]
	Limit (95% CL)		τ (theor.)	ref.
$BR(\overline{B}_s \rightarrow \mu^+ \mu^-)$	$< 5.8 \times 10^{-8}$		14%	[30]
m_h	> 114.4 GeV (91.0 GeV)		3 GeV	[31]
ζ_h^2	$f(m_h)$		negligible	[31]
sparticle masses	See table 4 in ref. [15].			

Table 2: Summary of the observables used in the analysis. Upper part: Observables for which a positive measurement has been made. $\delta(g-2)_\mu$ denotes the discrepancy between the experimental value and the SM prediction of the anomalous magnetic moment of the muon $(g-2)_\mu$. For central values of the SM input parameters used here, the SM value of $BR(\overline{B} \rightarrow X_s \gamma)$ is 3.11×10^{-4} , while the theoretical error of 0.21×10^{-4} includes uncertainties other than the parametric dependence on the SM nuisance parameters, especially on M_t and $\alpha_s(M_Z)^{\overline{MS}}$. For each quantity we use a likelihood function with mean μ and standard deviation $s = \sqrt{\sigma^2 + \tau^2}$, where σ is the experimental uncertainty and τ represents our estimate of the theoretical uncertainty (see [15] for details). Lower part: Observables for which only limits currently exist. The likelihood function is given in ref. [15], including in particular a smearing out of experimental errors and limits to include an appropriate theoretical uncertainty in the observables. m_h stands for the light Higgs mass while $\zeta_h^2 = g^2(hZZ)_{\text{MSSM}}/g^2(hZZ)_{\text{SM}}$, where g stands for the Higgs coupling to the Z and W gauge boson pairs.

3. Probability maps of NUHM parameters and observables

In this section we present some results from our global scans of the NUHM parameter space. To start with, in fig. 1 we plot joint 2D probability density functions (pdfs) for some combinations of the NUHM base parameters in the log prior case. First, in the left panel in the plane spanned by $m_{1/2}$ and m_0 we can see that the 68% total probability region (inner contour) is remarkably well confined to mostly a fairly low mass region of $m_{1/2} \lesssim 1$ TeV and $m_0 \lesssim 1.4$ TeV, where also the best fit points, marked by green triangles are located – we will discuss them below. Turning to the middle panel, we can see a preference for moderately large $\tan \beta \lesssim 40$, as well as for positive A_0 , although zero or negative values of A_0 are not excluded. In some sense the latter may even be favoured as indicated by the best fit points. Finally, the new parameters beyond the CMSSM exhibit interesting behaviour and, as we shall see, a strong prior dependence. With the log prior m_{H_u} is fairly poorly constrained while m_{H_d} favors rather low values. We will examine m_{H_u} and m_{H_d} in more detail below.

Coming back to $m_{1/2}$ and m_0 , we can see that, while the 68% total probability region

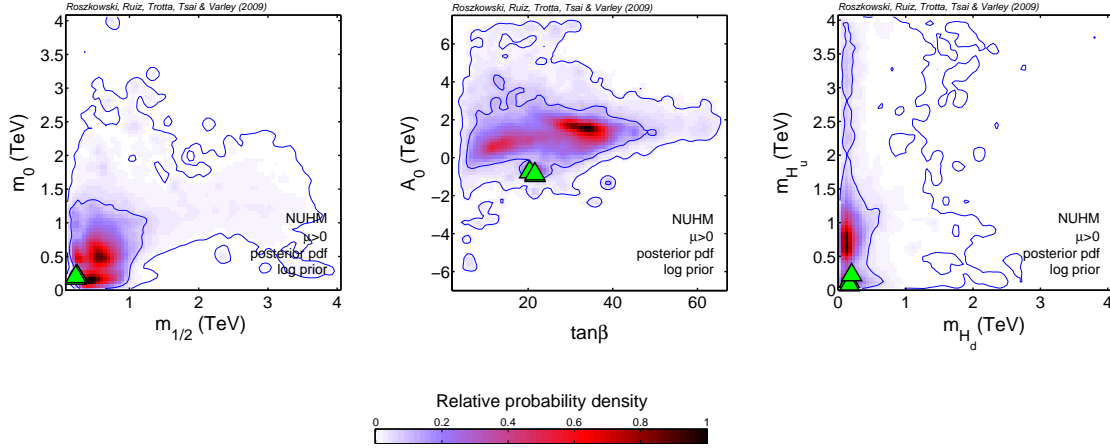


Figure 1: The 2D relative probability density functions in the planes spanned by three pairs of NUHM parameters: $(m_{1/2}, m_0)$, $(\tan\beta, A_0)$ and (m_{H_d}, m_{H_u}) for the log prior and for $\mu > 0$. The pdfs are normalised to unity at their peak. The inner (outer) blue solid contours delimit regions encompassing 68% and 95% of the total probability, respectively. All other basis parameters, both NUHM and SM ones, in each plane have been marginalized over (i.e., integrated out). Green triangles denote the three best fitting points.

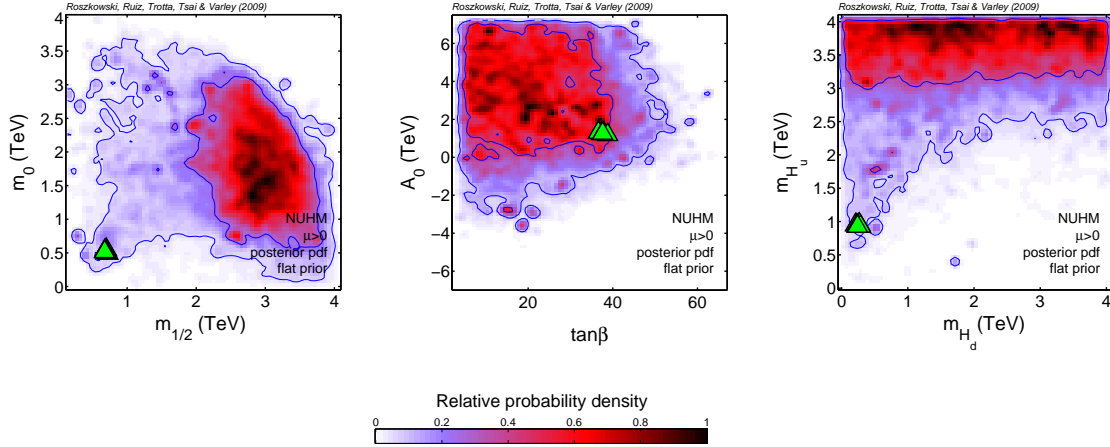


Figure 2: The same as in fig. 1 but for the flat prior. As explained in the text, the considerable shift in the probability density is largely due to a volume effect from the flat prior arising from the large number of samples at large mass for this choice of priors. The results obtained with log prior (fig. 1) are to be considered more robust as they are the ones where the probability density is in better agreement with the average quality of fit.

is well constrained, the 95% region (outer contour) is much wider and extends to much larger ranges of both parameters. This signals that the constraining power of the data is not sufficient to strongly confine the posterior. In order to examine this, in fig. 2 we plot the same quantities as in fig. 1 but assuming the flat prior. We find that the region of large $m_{1/2} \gtrsim 2$ TeV, as well as of $0.5 \text{ TeV} \lesssim m_0 \lesssim 3 \text{ TeV}$ (with a preference for $m_{1/2} \gtrsim m_0$)

is in this case much more prominent and actually favored from the point of view of the posterior. As we shall show below, this is actually largely due to a volume effect in the prior, for in fact the average χ^2 in the large mass region is relatively poorer than in the small mass region. The upper bound on the high probability regions of $m_{1/2}$ and m_0 mostly results from the adopted upper limit on m_{H_u} . The best fit points have also shifted upwards but not nearly as much and remain far away from the 68% total probability region. This suggests that the resulting picture suffers from the previously mentioned volume effect due to integrating over the additional dimensions: at large $m_{1/2}$ the fit to the data is moderate but there is a large volume of such points.² In Bayesian statistics such situations appear to be favored because of the large number of samples contained in the large volume implied by the choice of measure contained in the prior. Thus the flat prior appears to override the preference for the small mass region (where the average χ^2 is generally better), in the sense that it imposes a measure on parameter space that does not adequately explore the low mass region. For this reason below we will present results for that choice mostly in order to illustrate prior dependence, rather than by treating it on equal footing with the log prior. It should be kept in mind that the log prior results are the ones where the posterior distribution more fairly represents the actual quality of fit of the likelihood. It is expected that with better, more constraining data this prior dependence will be resolved and the posterior will become largely prior independent.

This approach is further justified by comparing the other two combinations of base parameters presented in figs. 1 and 2. In particular, with the flat prior the range of A_0 has much expanded, especially towards larger positive values. The 68% and 95% total probability ranges of $\tan\beta$ have actually shrunk somewhat but the best fit points have moved from around 20 in the log prior case to nearly 40. The favored ranges of the Higgs soft masses show an even stronger volatility with prior choice. While, as we have noted above, for the log prior m_{H_d} is rather strongly pushed toward lower values, well below 1 TeV, but m_{H_u} remains fairly unconstrained. In contrast, with the flat prior m_{H_u} shows strong preference for large values close to its upper limit while m_{H_d} is generally unconstrained. A proper understanding of this seemingly uncontrollable behavior will require some further investigation that we will conduct below. Nevertheless, this point illustrates the difficulty in reliably constraining both m_{H_u} and m_{H_d} with currently available data. On the other hand, the best fit points for both priors tend to agree more with the log prior posterior, which is another sign that this choice of prior leads to a posterior being better aligned with the high likelihood regions.

It is worth comparing the high probability regions of the NUHM with those for the analogous parameters in the CMSSM. The left two panels in figs. 1 and 2 are directly comparable with the corresponding panels in fig. 13 of [19]. The first point to remember

²To estimate the magnitude of this volume effect, recall that, for the flat prior, the volume encompassed by the mass range between e.g. 1 and 4 TeV is a factor 10^4 larger than between 100 and 400 GeV. For comparison, under the log prior the ratio of the volumes of the two regions is unity. Therefore, in order to completely override the prior volume via the likelihood, one would need at least a $\sim 4.3\sigma$ preference for the low mass region. Clearly, current data is not constraining enough to override the prior preference for large mass in this case.

is that prior dependence was already rather strong in the CMSSM and it should come as no surprise that in the NUHM, with two more free parameters, the 2D joint pdfs with all the other parameters marginalized over, show an even stronger dependence. Interestingly, in both models different regions of the corresponding parameters are typically favored. In the log prior case, in both the CMSSM and the NUHM, rather low $m_{1/2}$ and m_0 ranges are favored (a reflection of log prior’s preference for low masses), but actually different ones and selected by different physical mechanisms. In the CMSSM this is mostly the neutralino-stau coannihilation region of $m_0 \ll m_{1/2} \lesssim 1$ TeV [19] (plus a tiny vertical region of Z and h pole annihilation), while in the NUHM the analogous (mentioned above) “low-mass” ranges $m_{1/2} \lesssim 1$ TeV and $m_0 \lesssim 1.4$ TeV corresponds to the “bulk region” where A funnel annihilation play a dominant rôle. In both models, the favored ranges (and also best fit points) of $\tan\beta$ are rather moderate (although in the CMSSM very large values of around 55 are not excluded). Finally, A_0 in both models shows a mild preference for positive values.

In contrast, for the flat prior the difference between the overlapping CMSSM and NUHM parameters is much larger, which, again, is a reflection of the volume effect in both cases. In the CMSSM the focus point region (FP) [32] of large $m_0 \gtrsim m_{1/2}$ is favored (although with the stau coannihilation region still remaining allowed) [18, 19]. In contrast, in the NUHM a very different region of large $m_{1/2} \gg m_0$ is favored, as discussed above. Apart from the statistical reasons given above, the underlying physics is also different. In the CMSSM, the FP region is to a large extent favored by an interplay between the current SM prediction for and an experimental world average of $BR(\overline{B} \rightarrow X_s \gamma)$ [18, 19]. The case of the NUHM will be discussed shortly. Also, the strong preference for very large $\tan\beta \simeq 50 - 55$ in the CMSSM should be contrasted with significantly lower values of the parameter being favored in the NUHM. This may be because in the NUHM the large $\tan\beta$ regime affects strongly the running of the slepton masses via the Yukawa couplings which appear in the RG equations, making $Y_{\tau,b}$ large (and making Y_t small) which could lead to problems with EWSB or tachyonic sleptons [10].

In the NUHM with the flat prior, the high probability region of large $m_{1/2}$ in fig. 2 corresponds to the (lightest) neutralino χ being mostly higgsino. This can be seen in the right panel of fig. 3 where we plot the values of the χ gaugino fraction $Z_g = Z_{11}^2 + Z_{12}^2$ in the $m_{1/2}, m_0$ plane, where Z_{11}^2 is the bino fraction of the neutralino and Z_{12}^2 the wino fraction. We show three distinct regions: red dots correspond to a mostly higgsino state, $Z_g < 0.3$, green squares to a mixed state ($0.3 < Z_g < 0.7$) and blue diamonds to mostly gaugino neutralino, $Z_g > 0.7$. This is a new feature of the NUHM which distinguishes it from the CMSSM where the neutralino is mostly a bino (also in the FP where the higgsino component, while larger, still remains subdominant).³ Although in general a lighter higgsino-dominated LSP underproduces dark matter, this is not the case for heavy enough higgsinos. The significance of the higgsino LSP region clearly depends strongly on the assumed prior, which is evident by comparing the left and right panels of fig. 3 (and the corresponding left panels of figs. 1 and 2), but its presence is an interesting new feature of

³The possibility of higgsino-like LSP in the NUHM has also been noticed in [33] but not explored in more detail.

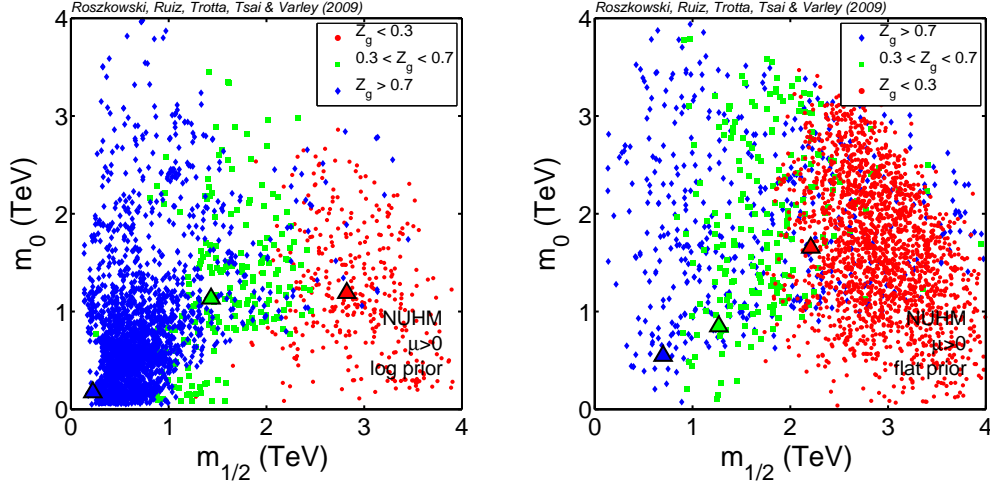


Figure 3: Values of the gaugino fraction $Z_g = Z_{11}^2 + Z_{12}^2$ in the plane of $(m_{1/2}, m_0)$ for samples uniformly selected from our MC chains obtained assuming the log prior (left panel) and the flat prior (right panel). The color coding is as follows: red dots correspond to $Z_g < 0.3$ (mostly higgsino), green squares to $0.3 < Z_g < 0.7$ and blue diamonds to $Z_g > 0.7$ (mostly gaugino). The triangles denote the best fit point for each cloud of samples of a given respective gaugino fraction (of corresponding color) taken separately. The overall best-fit is for both priors in the gaugino-like DM region.

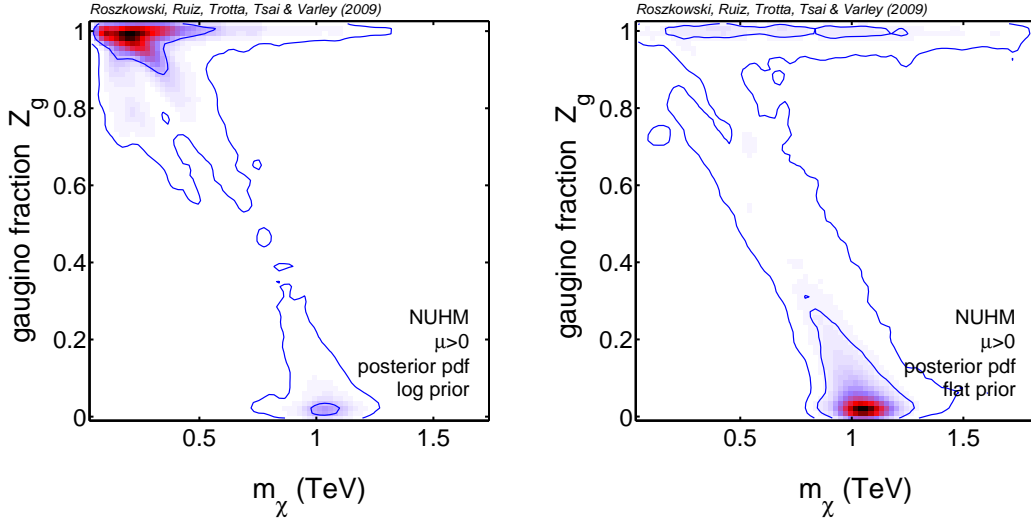


Figure 4: For the neutralino mass m_χ and its gaugino fraction Z_g we show the posterior for the log prior (left panel) and flat prior (right panel).

the phenomenology of the NUHM that is not present in the CMSSM. More quantitatively, we find for the log prior that the probability of the higgsino region is $\sim 12\%$, which increases

to $\sim 70\%$ for the flat prior case. Although the latter figure is strongly influenced by the volume effect, even in the more conservative case of a log prior we can still conclude that the higgsino DM region has a sizable probability in the NUHM (of order 10%). We can also investigate the behaviour of the χ^2 for each of the three regions separately and for both priors. We find that the overall best-fit is always to be found in the region where the LSP is mostly gaugino (blue samples in fig. 3), for both priors. However, the average χ^2 in each of the three clouds of samples is almost constant, which clearly shows that volume effects are at work and that the relative population of samples in the three regions is strongly influenced by the choice of prior.⁴

In order to examine in more detail the higgsino DM in the NUHM, in fig. 4 we present a 2D joint pdf in the neutralino mass and its gaugino fraction. The higgsino region is clearly pronounced at $m_\chi \sim 1$ TeV in the flat prior case but it is much less pronounced in the log prior case where the neutralino is mostly a bino. This will affect the ensuing predictions for DM searches, as we shall see later.

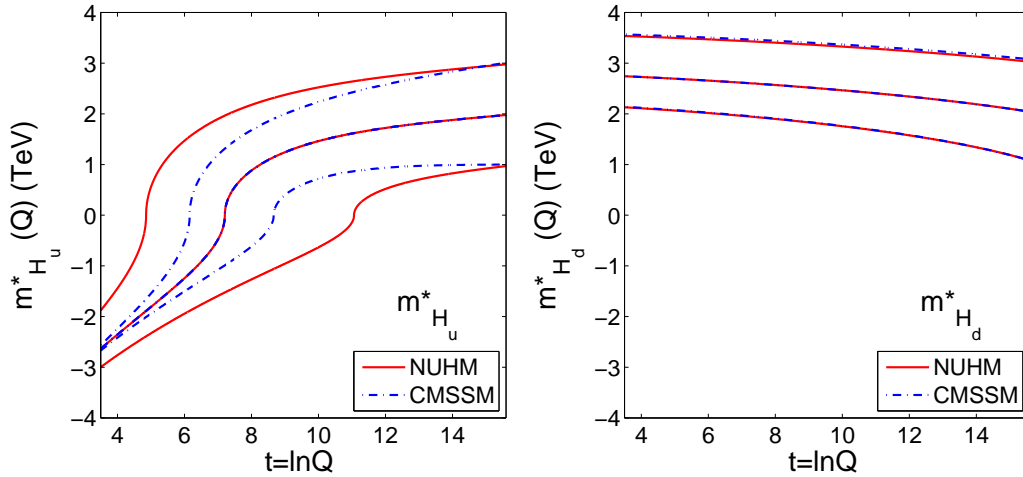


Figure 5: The running of $m_{H_u}^*(Q)$ (left panel) and $m_{H_d}^*(Q)$ (right panel) with the log of energy scale $t = \ln Q$. We take $A_0 = 4$ TeV, $m_{1/2} = 3$ TeV, $\tan \beta = 5$ and, in the NUHM case (red solid lines), $m_0 = 2$ TeV. In order to facilitate comparison with the CMSSM (blue dash-dotted lines), for each curve we initially set $m_{H_d} = m_{H_u}$ and then evolve differently for each model. In the CMSSM, for each curve we take $m_0 = m_{H_d} = m_{H_u}$, which is why the middle curves overlap.

For further discussion it will be convenient to introduce the running parameters $m_{H_u}^*(Q)$ and $m_{H_d}^*(Q)$, where Q is the energy scale, defined as

$$m_{H_{u,d}}^*(Q) = \text{sgn} \left(m_{H_{u,d}}^2(Q) \right) |m_{H_{u,d}}^2(Q)|^{1/2}. \quad (3.1)$$

⁴We have also investigated the impact of the constraint coming from the anomalous magnetic moment of the muon, $\delta(g-2)_\mu$, which has been shown to be in some tension with $b \rightarrow s\gamma$ [19]. If one removes $\delta(g-2)_\mu$ from the analysis, the average χ^2 and the best-fit values for the three different region become very close to each other. This shows that the fit is being driven to a large extent by the (somewhat controversial) $\delta(g-2)_\mu$ constraint. As such, one has to exercise some care in interpreting the ensuing conclusions.

Since in the RGEs the running Higgs soft mass parameters $m_{H_u}(Q)$ and $m_{H_d}(Q)$ appear only in squares, which can become negative, the parameters $m_{H_{u,d}}^*(Q)$ are convenient to deal with in the sense that they adequately reflect both the magnitude and the sign of the respective parameters $m_{H_{u,d}}^2(Q)$. In particular, the quantities $m_{H_{u,d}}^*$, without any arguments, will denote the respective running quantities evaluated at $Q = M_{\text{SUSY}}$,

$$m_{H_{u,d}}^* \equiv m_{H_{u,d}}^*(Q = M_{\text{SUSY}}). \quad (3.2)$$

We are now in the position to address the apparent strong prior dependence of m_{H_u} and m_{H_d} in figs. 1 and 2. This feature, and also the presence of the higgsino LSP, originate from another new interesting feature of the NUHM parameter space which is the existence of a mild focussing effect in the RG running of m_{H_u} , akin to that in the CMSSM [32]. The effect is illustrated in fig. 5 where red solid lines show the running of the NUHM parameters $m_{H_u}^*(Q)$ (left panel) and $m_{H_d}^*(Q)$ (right panel) with the log of energy scale $t = \ln Q$. For each case we take $A_0 = 4$ TeV, $m_{1/2} = 3$ TeV and $\tan\beta = 5$. In order to facilitate comparison with the CMSSM (blue dash-dotted lines), for each curve we initially set $m_{H_d} = m_{H_u}$ and then evolve differently in each model. In the NUHM we fix also $m_0 = 2$ TeV while in the CMSSM, for each curve we take $m_0 = m_{H_d} = m_{H_u}$, which is why the curves in the middle case overlap. One can see that, in the NUHM the running of m_{H_u} is stronger for larger GUT values of the parameter, but it is not as strong as in the CMSSM.

As a result, we can see some “squeezing” of $m_{H_u}^*$ compared to the GUT values m_{H_u} , while this is not the case with the H_d soft mass parameter. This is shown in fig. 6 where, in the flat prior case (right panel) the fairly narrow inner 68% total probability region of $m_{H_u}^*$ between some -1 TeV and -0.5 TeV corresponds to large values of m_{H_u} (compare fig. 2), close to the assumed upper limit of the prior, nearly independently of the H_d soft mass parameter. It is clear from this that $m_{H_u}^*$ is to a large extent constrained by the focussing effect in the RG running, while the most probable ranges of $m_{H_d}^*$ are more prior dependent. On the other hand, in the log prior case m_{H_u} prefers to be smaller than for the other prior (compare right panels of figs. 1 and 2) basically in order to arrive at bino-like neutralino with correct relic density, as we will show below. In this case, however, m_{H_d} is confined to preferably fairly small values ($\lesssim 2$ TeV) as otherwise one ends up with tachyonic sleptons. (We can also again see that, in the log prior case the high probability region agrees rather well with the best fit points, while this is not so with the flat priors.) The corollary to this is that, in general we have more freedom in obtaining a phenomenologically desired range of values at the electroweak scale by appropriately choosing m_{H_u} at the GUT scale. Clearly that is not so in the CMSSM as one can never attain smaller μ here due to the stronger FP behaviour essentially focusing to nearly one point at the EW scale. The two distinct branches visible in fig. 6 correspond to two distinct neutralino regimes, as shown in fig. 7. In the horizontal branch the neutralino is mostly a higgsino (red dots) while the other, an inverted ‘V’ shaped region around $m_{H_d}^* = 0$ gives us a mostly bino (blue diamonds).

Above the reach of current collider limits, the high probability regions of m_{H_u} , m_{H_d} and the other soft parameters are primarily determined by requiring the correct dark matter

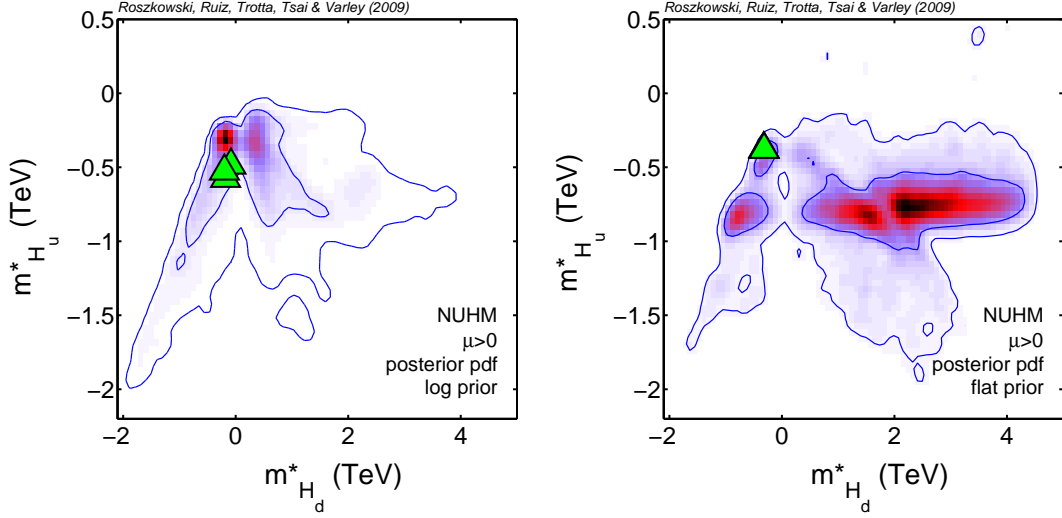


Figure 6: For $m_{H_u}^*$ and $m_{H_d}^*$ we show the posterior for the log prior (left panel) and flat prior (right panel).

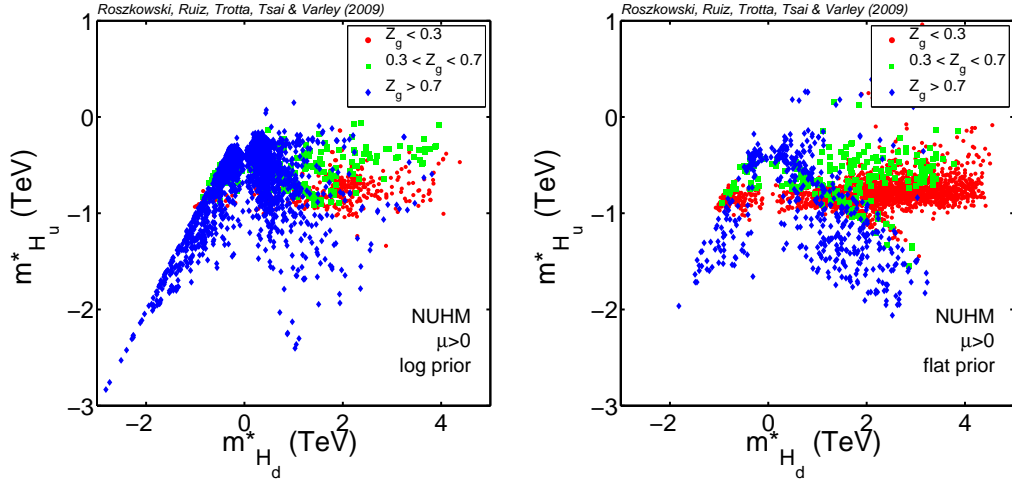


Figure 7: Values of the gaugino fraction Z_g in the plane of $(m_{H_d}^*, m_{H_u}^*)$ for samples uniformly selected from our MC chains obtained assuming the log prior (left panel) and the flat prior (right panel). The color coding is as follows: red dots correspond to $Z_g < 0.3$ (mostly higgsino), green squares to $0.3 < Z_g < 0.7$ and blue diamonds to $Z_g > 0.7$ (mostly gaugino).

abundance.⁵ It is well known that, in order to satisfy this constraint, the LSP neutralino can either be mostly bino-like (like in the CMSSM) if the bino soft mass $M_1 < |\mu|$, or else a sufficiently heavy higgsino-like state with $|\mu| < M_1$. With flat priors imposed on the soft masses it is the second choice that is primarily realized in the NUHM, because,

⁵Exploratory runs with the constraint switched off yield much wider ranges of parameters.

as explained above, by starting with large enough m_{H_u} at the GUT scale one arrives, via the mild focusing effect (see fig. 5) at less negative values of $m_{H_u}^*$ at the EW scale. In the limit $|m_{H_d}^*| \ll |m_{H_u}^*|$ and large enough $\tan\beta$, eq. (1.2) would imply $\mu \simeq |m_{H_u}^*|$. In reality, in the NUHM this limit is often violated and as a result μ comes out somewhat larger. In any case, with flat priors one obtains small enough values of μ and higgsino dark matter. On the other hand, $m_\chi \simeq |\mu|$ has to be large enough to give an acceptable relic density, as mentioned before. Numerically, this leads to $\mu \gtrsim 0.8$ TeV, which translates (via $0.4 m_{1/2} \simeq M_1 > |\mu|$) to $m_{1/2} \gtrsim 2$ TeV; see the left panel of fig. 2. The second EWSB condition, eq. (1.3), then implies the approximate relation $m_A^2 \simeq m_{H_d}^{*2} + \mu^2$ which we have checked numerically to hold.

The condition $\mu \gtrsim 0.8$ TeV is reflected as the left side of an inner (68%) vertical contour in the right panel of fig. 8 where we show the joint 2D posterior in the plane (μ, m_A) . On the other side, as μ increases, so does $\Omega_\chi h^2$ which quickly becomes unacceptably large. As a result one finds a strong concentration at $\mu \simeq 1$ TeV, corresponding to higgsino LSP.

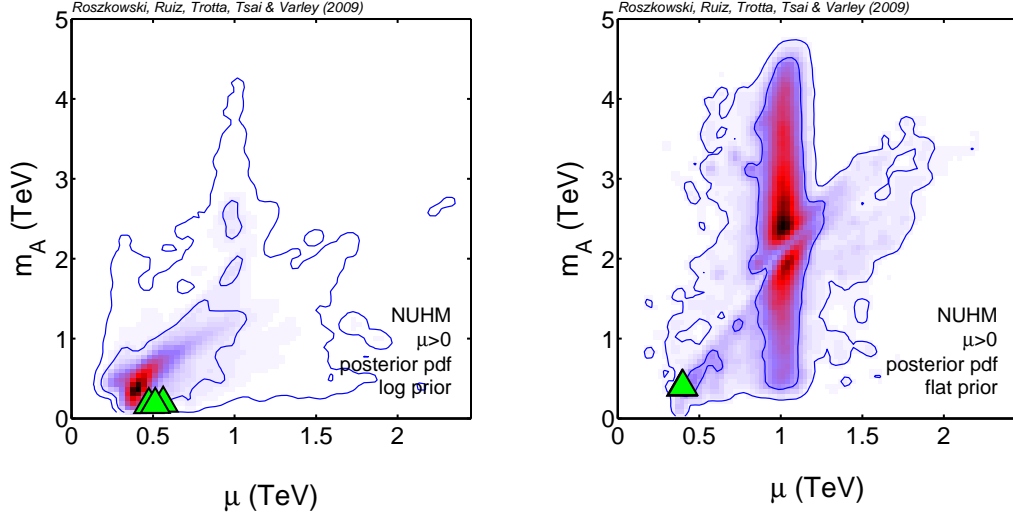


Figure 8: For μ and m_A we show the joint 2D posterior for the log prior (left panel) and flat prior (right panel).

The higgsino LSP at $m_\chi \simeq |\mu| \simeq 1$ TeV is further emphasized in fig. 9 where we show values of the gaugino fraction Z_g in the plane of (m_χ, m_A) for samples uniformly selected from our MC chains obtained assuming the log prior (left panel) and the flat prior (right panel). The color coding is as before: red dots correspond to $Z_g < 0.3$ (mostly higgsino), green squares to $0.3 < Z_g < 0.7$ and blue diamonds to $Z_g > 0.7$ (mostly gaugino). The vertical higgsino region at $m_\chi \simeq 1$ TeV is strongly pronounced for the flat prior although is also visible in the log prior case whose impact in pushing masses to lower values is again visible.

On the other hand, the diagonal branch in fig. 9 corresponds to the second way of arriving at the correct relic density, namely via bino-like neutralino which is clearly also

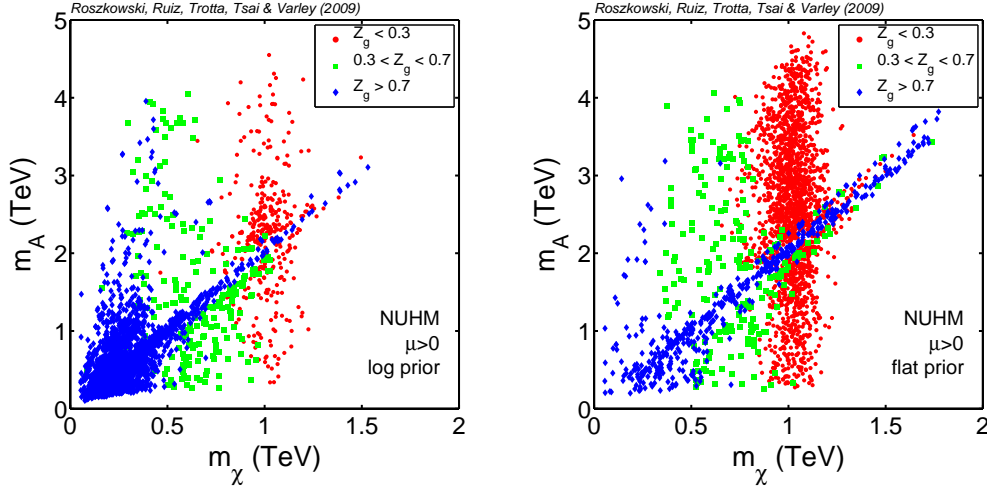


Figure 9: Values of the gaugino fraction Z_g in the plane of (m_χ, m_A) for samples uniformly selected from our MC chains obtained assuming the log prior (left panel) and the flat prior (right panel). The color coding is as follows: red dots correspond to $Z_g < 0.3$ (mostly higgsino), green squares to $0.3 < Z_g < 0.7$ and blue diamonds to $Z_g > 0.7$ (mostly gaugino).

realized in the NUHM. In this case the LSP mass m_χ extends over a range of values and the correct relic density is achieved via a A resonance when $m_A \simeq 2m_\chi$. This feature can be seen in both panels of fig. 9. It also explains a kink at $\mu \simeq 1$ TeV in the right panel of fig. 8.

In the case of the log prior, with its built-in emphasis on low masses, the preference for the bino and the higgsino DM regions in some sense gets interchanged, as can be seen by comparing the left and right panels of the above figures. The effect of the log prior is twofold. Firstly, it serves to put the emphasis to low $m_{1/2}$ where, even if one can achieve $\mu < M_1$, the higgsino will be too light to give the correct relic density. Coupled with this, the emphasis on the low mass region of m_{H_u} also plays a rôle: if one starts with too low values of m_{H_u} at the GUT scale, one arrives at too large values of $|\mu|$ and an incorrect relic abundance. The only way to satisfy the cosmological constraint is then to rely on the bino-like DM which requires small enough M_1 and therefore $m_{1/2}$. This is precisely what one can see in fig. 1 and subsequent figures showing the log prior case.

In summary, the parameters of the NUHM exhibit a rather complex structure. Clearly the two priors adopted here give us sizeably different results, but even the strong preference for the low mass region encoded in the log prior is not sufficient to completely kill off the much bigger regions of large $m_{1/2}$ and m_0 which are strongly favored by the flat prior. In some senses we have two distinct regimes here. One has a 1 TeV higgsino neutralino and corresponds mostly to large values of the soft mass parameters, whilst the other is more similar to the situation seen in the CMSSM, with bino dark matter and a lighter spectrum.

4. Collider signatures

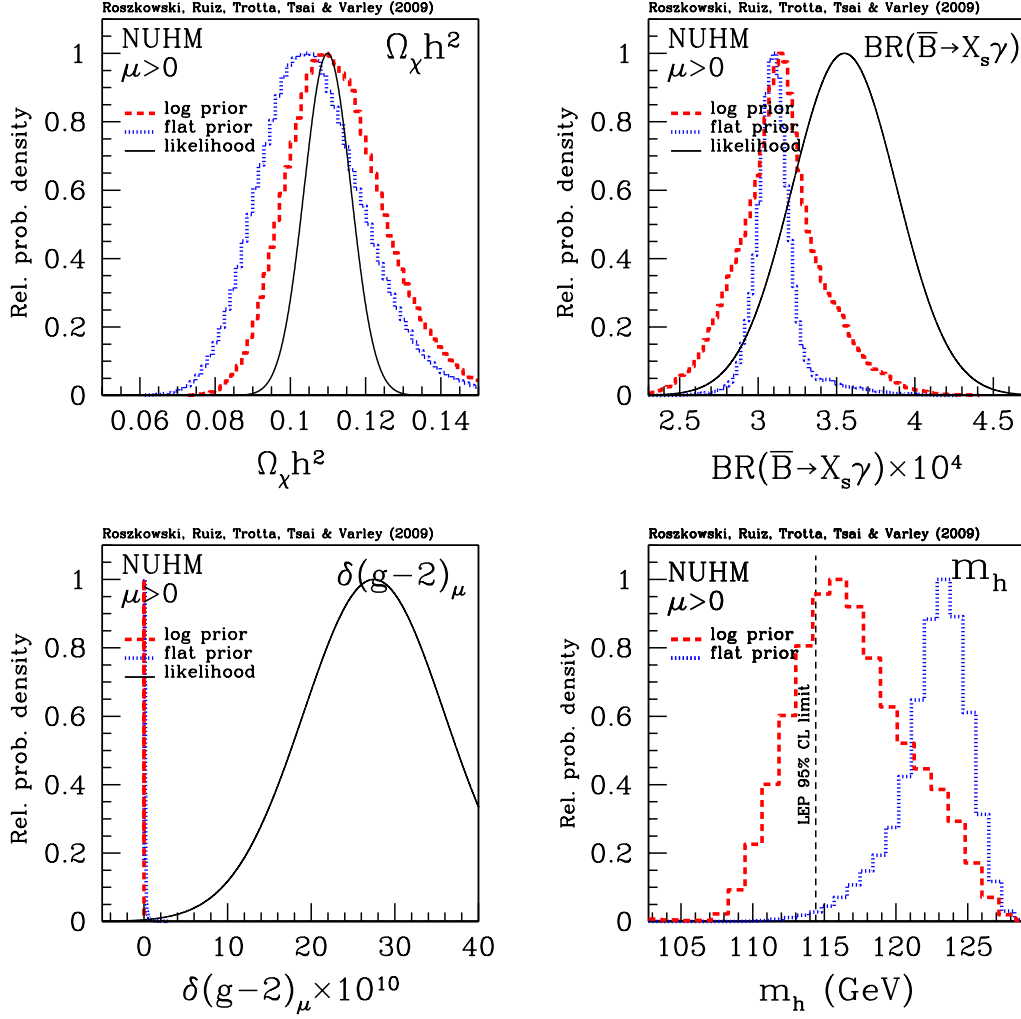


Figure 10: The 1D relative probability densities for $\Omega_\chi h^2$ (upper left panel), $BR(\bar{B} \rightarrow X_s \gamma)$ (upper right panel), $\delta(g-2)_\mu$ (lower left panel) and the light Higgs mass m_h (lower right panel). In each panel we show the posterior for the flat prior (dotted blue) and the log prior (long-dashed red) and the likelihood function (solid black).

Now we turn to discussing some of the observables that play a key rôle in determining the favored regions of NUHM parameter space and also discuss some implications for the light Higgs, neutralino, chargino and gluino mass spectra.

To start with, shown in fig. 10 are the 1D posterior pdfs for the four key constraints on the model: the neutralino relic abundance $\Omega_\chi h^2$, $BR(\bar{B} \rightarrow X_s \gamma)$, the SUSY contribution to $(g-2)_\mu$ and the light Higgs mass m_h . It is clear that a tight WMAP constraint on $\Omega_\chi h^2$

Parameter	Best fit (log)	Best fit (flat)	Best fit w/o $(g-2)_\mu$ (log)
$m_{1/2}$	224 GeV	698 GeV	1.47 TeV
m_0	174 GeV	547 GeV	3.22 TeV
m_{H_u}	129 GeV	959 GeV	3.55 TeV
m_{H_d}	162 GeV	265 GeV	1.82 TeV
A_0	-755 GeV	1.23 TeV	3.62 TeV
$\tan \beta$	20.3	37.8	35.8
μ	474 GeV	392 GeV	638 GeV
m_A	469 GeV	218 GeV	484 GeV
$m_{H_d}^*$	-486 GeV	-375 GeV	-474 GeV
$m_{H_u}^*$	-83.4 GeV	-321 GeV	-373 GeV
$\Omega_\chi h^2$	0.111	0.112	0.104
$BR(\overline{B} \rightarrow X_s \gamma)$	3.53×10^{-4}	3.50×10^{-4}	3.53×10^{-4}
$BR(\overline{B}_s \rightarrow \mu^+ \mu^-)$	7.4×10^{-8}	4.7×10^{-8}	3.79×10^{-8}
$BR(\overline{B}_u \rightarrow \tau \nu)$	1.1×10^{-4}	0.12×10^{-4}	8.41×10^{-4}
$\delta(g-2)_\mu$	27.1×10^{-10}	12.4×10^{-10}	1.06×10^{-10}
m_h	115.6 GeV	115.9 GeV	121.0 GeV
m_χ	88.6 GeV	283 GeV	618 GeV
$m_{\chi_1^\pm}$	172.3 GeV	392 GeV	664 GeV
$m_{\tilde{g}}$	553 GeV	1.57 TeV	3.28 TeV
χ^2	6.99	10.93	6.22

Table 3: A table showing the values of various parameters for the best fitting point in both the log and flat prior case, as well as the effect of removing the $(g-2)_\mu$ constraint on the best fitting (i.e., log prior) point.

in the likelihood is reasonably well matched by the shape of the 1D pdfs for both priors. Likewise, the 1D pdfs of $BR(\overline{B} \rightarrow X_s \gamma)$ for both priors show a rather strong preference for basically the SM value of the observable, although, naturally, with the log prior we find a larger tail of bigger values, much closer to the experimental average. Also, the SUSY contribution to $(g-2)_\mu$ comes out rather tiny, resulting in $\delta(g-2)_\mu \simeq 0$ for both priors that we examined. This is an interesting characteristic feature which we have already seen in the case of the CMSSM [18, 19]. Finally, the posterior for m_h shows a somewhat stronger prior dependence, although the case of the log prior does favor lower m_h values and allows for a wider spread due to its built-in preference for lower values of basis parameters. Interesting, unlike in the CMSSM, the lightest Higgs is not necessarily SM-like and therefore the 95% LEP lower bound on SM Higgs mass should only be considered as indicative. We will investigate the Higgs sector of the model in more detail elsewhere.

Generally, it is interesting to note that posterior pdfs for these observables do not vary wildly with differing prior, although the log prior in general seems to lead to somewhat less strongly peaked posteriors. Finally, it is remarkable that even in this rather different model, the pdfs for both set of priors are fairly similar to those in the CMSSM [18, 19].

In table 3 we present best fit values for the NUHM base parameters and for a number of

quantities of particular interest, as well as the χ^2 values. Clearly, the log prior does provide a better χ^2 than the flat prior and in this sense the log prior does look more appropriate to explore the properties of the model. The best fitting point in the flat prior case is included for contrast and to illustrate the larger values for the base mass parameters and derived spectrum. Back to the log prior case, it is interesting to note that although removing the $(g-2)_\mu$ constraint does not spectacularly improve the fit, it does move the best fit for the base parameters and corresponding masses to much higher values. On the other hand, removing the $(g-2)_\mu$ constraint brings the best fit value for the flat prior back in line with the value obtained for the log prior, thus giving a marked improvement over the case where it is included. That said, the main “indirect” observables $\Omega_\chi h^2$, $BR(\overline{B} \rightarrow X_s \gamma)$ and $BR(\overline{B}_s \rightarrow \mu^+ \mu^-)$ (although not $(g-2)_\mu$) remain fairly similar, in line with what is observed for the pdfs.

On the other hand, the impact of the priors on superpartner masses is quite strong, with a whole slew of heavy particles in the flat prior case being strongly contrasted with the low mass regions (and hence lighter spectra) preferred by the log prior. This point is illustrated in fig. 11 where we present the 1D posterior pdfs for the lightest neutralino (left panel), the lighter chargino (middle panel) and the gluino (right panel). This provides further evidence that the data is not yet good enough to properly constrain the model (as was already the case in CMSSM [19]) and as such care must be taken with the results. In particular, LHC prospects for detecting the gluino, up to some 2.7 TeV, can be considered either very good or very poor depending on the prior.

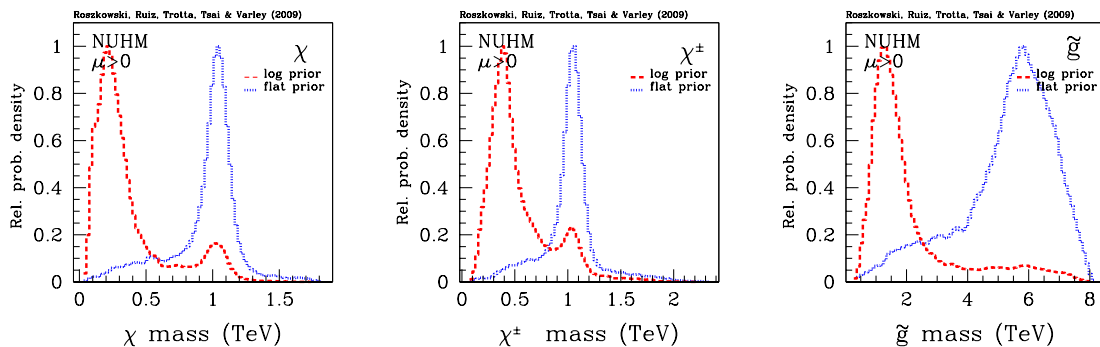


Figure 11: The 1D relative probability densities for the mass of the lightest neutralino m_χ (left panel), the lightest chargino m_{χ^\pm} (middle panel) and the gluino $m_{\tilde{g}}$ (right panel). In each panel we show the posterior for the flat prior (dotted blue) and the log prior (long-dashed red).

5. Dark matter signatures

In this section we will examine implications for the detection of the lightest neutralino assumed to be the DM in the Universe. We will consider both direct detection via its elastic scatterings with targets in underground detectors, as well as indirect signatures of neutralino pair annihilation resulting in an additional component of diffuse gamma

radiation from the Galactic center and of positron flux from the Galactic halo (see [34] instead for a recent analysis of the detection prospects for the gamma-ray flux from nearby dwarf galaxies in the context of the CMSSM). The underlying formalism for both direct and indirect search modes can be found in several sources. (See, e.g., [36, 35, 37, 38].) In our analysis we have followed the procedure as well as hadronic matrix elements inputs as presented in our earlier work [15, 18, 39]. Some investigations into this area in the case of non-universality have also been done in the literature, see for example ref. [7, 40].

To start with, in fig. 12 we present 2D posterior pdfs in the usual plane spanned by the spin-independent cross section σ_p^{SI} and the neutralino mass m_χ . The left (right) panel corresponds to the log (flat) prior. For comparison, some of the most stringent 90% CL experimental upper limits are also marked [41, 42, 43, 44, 45, 46], although they have not been imposed in the likelihood, as before in our studies of the CMSSM. As previously with superpartner masses, we can see a strong prior dependence, with the log prior generally favoring lower neutralino masses and therefore larger cross-sections. For the flat prior, in contrast, there is a well pronounced region of high probability in the higgsino LSP region of $m_\chi \simeq 1$ TeV, as we discussed above, which is present but less emphasized in the log prior case. The prior dependence is certainly somewhat discomforting, although it is merely a reflection of the model being unconstrained by the currently available data. Nevertheless, the larger 95% total probability regions (outer contours) are actually more similar. In any case, we note that in both cases the 68% regions of total probability (inner contours) correspond to $\sigma_p^{SI} \gtrsim 10^{-10}$ pb which means that, independently of the prior, the direct DM detection predictions of the model will be basically completely explored by current and especially future 1-tonne detectors whose sensitivity reach is likely to be of that order or better.

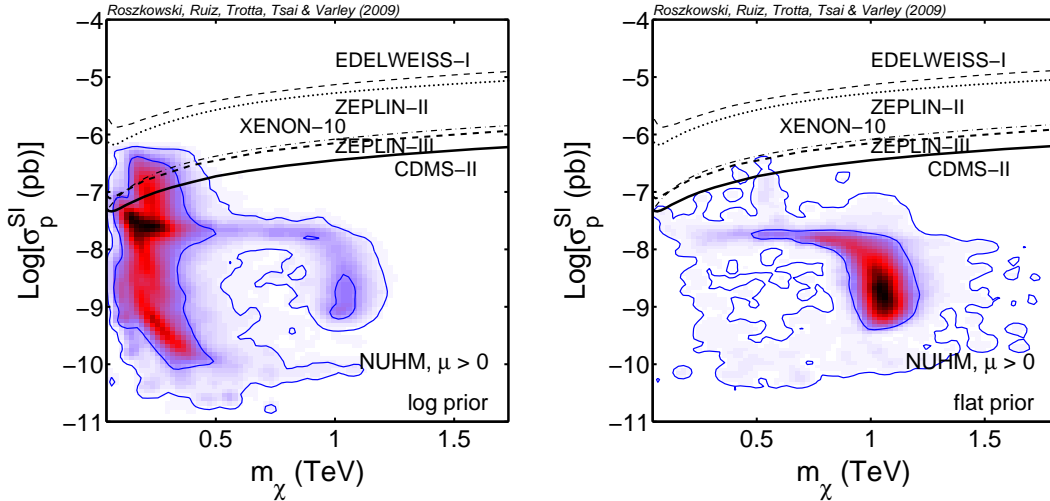


Figure 12: For the dark matter spin-independent cross section σ_p^{SI} vs. the neutralino mass m_χ we show the 2D relative probability density for the log prior (left panel) and the flat prior (right panel).

Next we discuss some indirect detection modes of much current interest. We follow the formalism and procedure outlined in ref. [39] which we briefly summarize here for completeness. In our numerical analysis we rely on DarkSusy [21] to compute the fluxes. To start with, we compute the total γ -ray flux Φ_γ produced by dark matter annihilations in the Galactic halo,

$$\Phi_\gamma(\Delta\Omega) = \int_{E_{\text{th}}}^{m_\chi} dE_\gamma d\Phi_\gamma/dE_\gamma(E_\gamma, \Delta\Omega), \quad (5.1)$$

where the cone $\Delta\Omega$ is centered on the direction ψ and the integration goes over the range of photon energies from an energy threshold E_{th} up to m_χ . The differential diffuse γ -ray flux arriving from a direction at an angle ψ from the Galactic center (GC) is given by

$$\frac{d\Phi_\gamma}{dE_\gamma}(E_\gamma, \psi) = \sum_i \frac{\sigma_i v}{8\pi m_\chi^2} \frac{dN_\gamma^i}{dE_\gamma} \int_{\text{l.o.s.}} dl \rho_\chi^2(r(l, \psi)), \quad (5.2)$$

where $\sigma_i v$ is a product of the WIMP pair-annihilation cross section into a final state i times the pair's relative velocity and dN_γ^i/dE_γ is the differential γ -ray spectrum (including a branching ratio into photons) following from the state i . Here we consider contributions from the continuum (as opposed to photon lines coming from one loop direct neutralino annihilation into $\gamma\gamma$ and γZ), resulting from cascade decays of all kinematically allowed final state SM fermions and combinations of gauge and Higgs bosons. The integral is taken along the line of sight (l.o.s.) from the detector. It is convenient to separate factors depending on particle physics and on halo properties by introducing the dimensionless quantity $J(\psi) \equiv (1/8.5 \text{ kpc}) (0.3 \text{ GeV/cm}^3)^2 \int_{\text{l.o.s.}} dl \rho_\chi^2(r(l, \psi))$ [47]. The flux is further averaged over the solid angle $\Delta\Omega$ representing the acceptance angle of the detector, and one defines the quantity $\bar{J}(\Delta\Omega) = (1/\Delta\Omega) \int_{\Delta\Omega} J(\psi) d\Omega$. Since we are interested in the Galactic center, we set $\psi = 0$.

The flux from the GC critically depends on the dark matter halo profile at small Galactic radius r where dark matter density is thought to be largest. In this analysis we consider a generic NFW model [48], as done previously in [39], but in addition also include a model of Klypin, et al., in [49]. It is based on the NFW model but it is fitted to the data from the Milky Way and takes into account the effect of angular momentum exchange between baryons and dark matter, and in this sense may be considered as more applicable to our Galaxy. The inner radius density profile for the Klypin, et al., model is $\sim r^{-1.8}$ which is quite a bit steeper than the NFW one with r^{-1} . Close to solar radius both models become quite similar.

In fig. 13 we present our predictions for the diffuse γ -ray flux Φ_γ produced by dark matter annihilation in the Galactic center *vs.* the neutralino mass m_χ for the two halo models. We also assume a conservative energy threshold $E_{\text{th}} = 10 \text{ GeV}$ and $\Delta\Omega = 10^{-5} \text{ sr}$ to match Fermi's resolution. We show the 2D relative probability density for the log prior (left panel) and the flat prior (right panel). For the Klypin, et al., model both the 68% and the 95% total probability ranges (inner and outer contours, respectively) are shown, while for the NFW only the 68% regions are plotted for comparison. Fermi's reach with one year of data is also indicated (horizontal black/dashed line [50]). For each prior the fluxes

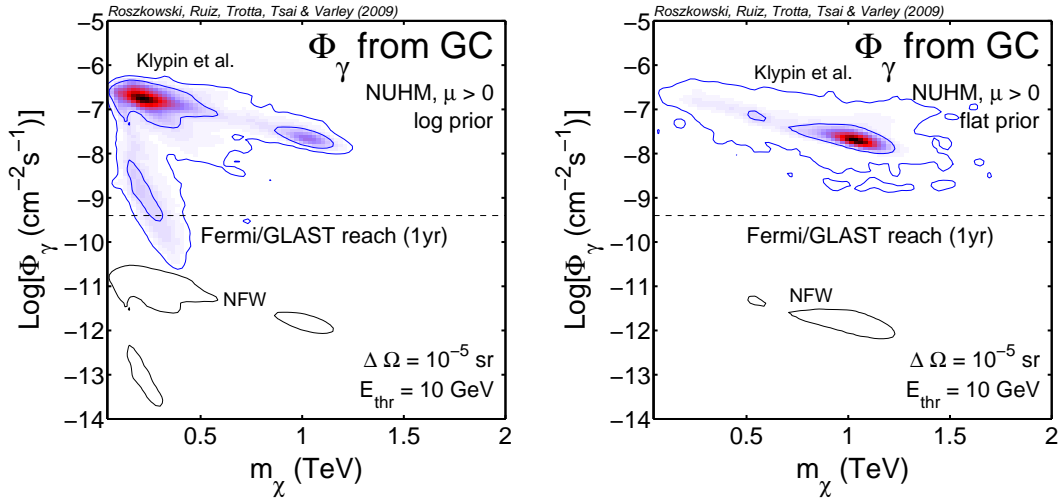


Figure 13: The diffuse γ -ray flux Φ_γ produced by dark matter annihilation in the Galactic center *vs.* the neutralino mass m_χ for some popular halo models. We show the 2D relative probability density for the log prior (left panel) and the flat prior (right panel). Klypin model (right panel).

are somewhat different, although in the same ballpark. The emerging picture is actually fairly similar to the CMSSM [39]. In particular, it is clear that the largest uncertainty in assessing Fermi's prospects for detecting a signal in this model lies in the cusiness of the dark matter halo profile at small radii. If the profile is a steep as in the Klypin, et al., model, then Fermi's prospects in this mode are very good, unlike for less cuspy models, like the NFW one.

Finally we present the NUHM's predictions for positron flux from neutralino dark matter annihilation in the local halo. Once produced, positrons propagate through the Galactic medium and their spectrum is distorted due to synchrotron radiation and inverse Compton scattering at high energies, bremsstrahlung and ionization at lower energies. The effects of positron propagation are computed following a standard procedure described in [51, 52], by solving numerically the diffusion-loss equation for the number density of positrons per unit energy $dn_{e^+}/d\varepsilon$. The diffusion coefficient is parameterized as $K(\varepsilon) = K_0(3^\alpha + \varepsilon^\alpha)$, with $K_0 = 2.1 \times 10^{28} \text{ cm}^2\text{sec}^{-1}$, $\alpha = 0.6$ and $\varepsilon = E_{e^+}/1 \text{ GeV}$, mimicking re-acceleration effects. The energy loss rate is given by $b(\varepsilon) = \tau_E \varepsilon^2$, with $\tau_E = 10^{-16} \text{ sec}^{-1}$, and we describe the diffusion zone (i.e., the Galaxy) as an infinite slab of height $L = 4 \text{ kpc}$, with free escape boundary conditions. Changes in the above positron propagation model, especially $K(\varepsilon)$ (see, e.g., [53, 52]), can potentially lead to variations by a factor of 5 to 10 in the spectral shape at low positron energy, $E_{e^+} \lesssim 20 \text{ GeV}$ [54]. Most high-energy positrons, on the other hand, originate from the local neighborhood the size of a few kpcs [52, 55], and their flux is less dependent of the halo and propagation dynamics. In order to reduce the impact of solar winds and magnetosphere effects on the model's predictions, it is useful to consider the positron fraction, defined as $\Phi_{e^+}/(\Phi_{e^+} + \Phi_{e^-})$, where Φ_{e^+} is the positron differential flux from WIMP annihilation, while Φ_{e^-} is the background electron

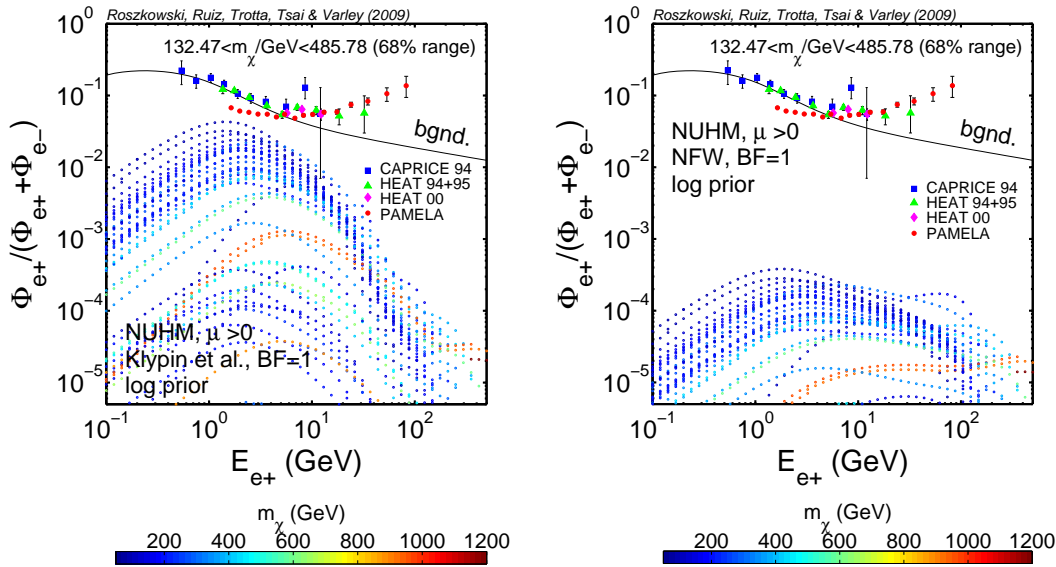


Figure 14: Predicted positron flux fraction produced by dark matter annihilation in the Galactic halo *vs.* the positron energy E_{e+} , assuming log priors and the boost factor $BF=1$, for the Klypin, et al., model (left panel) and the NFW model (right panel).

flux. For background e^- and e^+ fluxes we follow the parametrization adopted in ref. [52] from ref. [53].

In fig. 14 we present the positron flux fraction produced by dark matter annihilation in the Galactic halo *vs.* the positron energy E_{e+} for the two halo models considered above and for the log prior case. (The flat prior case is not qualitatively different.) Also included are the relevant experimental data [56, 57], including the recent Pamela result. It is clear that supersymmetric dark matter in the models like the NUHM (and also the CMSSM [39]) falls far short of reproducing the Pamela result. This would remain true even if one would be prepared to consider an unlikely existence of very dense local DM clumps for which the boost factor (BF) would be unrealistically high, $\sim 10^3$. Although a more refined analysis fitting signal and background simultaneously would be required to draw more quantitative conclusions, it is clear that the spectrum predicted by the NUHM appears to have a very different energy dependence from the flux observed by Pamela. This is not necessarily a problem for the NUHM, and other unified SUSY models like the CMSSM, as long as their signal remains below the observed flux, since a more conventional astrophysical explanation in terms of pulsar radiation may be entirely sufficient to account for Pamela observations [58].

6. Conclusions

The MCMC scan and Bayesian analysis of the Non-Universal Higgs Model performed in this paper reveal a remarkably rich and complex structure of its parameter space. While the properties of the model are in some aspects fairly similar to the CMSSM, we have

found several interesting differences. Perhaps the biggest one is the existence of higgsino-like dark matter with a mass close to 1 TeV, with a minimum probability of about $\sim 10\%$. This feature seems quite robust, as our exploratory scans with wider ranges of soft masses have confirmed, although the details are quite strongly prior dependent. The higgsino dark matter results from having more parameters than in the CMSSM but also from the focusing effect being less strong than in that model.

In terms of observational consequences at colliders, the NUHM actually appears rather similar to the CMSSM, which will make it difficult to experimentally distinguish the two models. Again, the best prospects may be provided by finding in direct detection searches a ~ 1 TeV dark matter WIMP, since such a case in the CMSSM is highly unlikely [18, 19]. Fermi's prospects for probing the model strongly depend on the cuspidity of the dark matter profile in the Galactic center while positrons produced in dark matter annihilation remain well below the Pamela result.

Acknowledgments

LR is partially supported by the EC 6th Framework Programmes MRTN-CT-2004-503369 and MRTN-CT-2006-035505. RRdA is supported by the project PARSIFAL (FPA2007-60323) of the Ministerio de Educación y Ciencia of Spain. TV is supported by STFC. The authors would like to thank the European Network of Theoretical Astroparticle Physics ENTApP ILIAS/N6 under contract number RII3-CT-2004-506222 for financial support. This project benefited from the CERN-ENTApP joint visitor's programme on dark matter, 2-6 February 2009. The use of the Iceberg computer cluster at the University of Sheffield is gratefully acknowledged.

References

- [1] See, e.g., H. E. Haber and G. L. Kane, *The Search for Supersymmetry: Probing Physics Beyond the Standard Model* *Phys. Rept.* **117** (1985) 75;
S. P. Martin, *A Supersymmetry Primer*, hep-ph/9709356.
- [2] G. L. Kane, C. F. Kolda, L. Roszkowski and J. D. Wells, *Study of constrained minimal supersymmetry*, *Phys. Rev. D* **49** (1994) 6173 [hep-ph/9312272].
- [3] T. Blazek, R. Dermisek and S. Raby, *Predictions for the Higgs and supersymmetry spectra from $SO(10)$ Yukawa unification with μ greater than 0*, *Phys. Rev. Lett.* **88** (2002) 111804 [hep-ph/0107097]; *Yukawa unification in $SO(10)$* , *Phys. Rev. D* **65** (2002) 115004 [hep-ph/0201081].
- [4] R. Dermisek, S. Raby, L. Roszkowski and R. Ruiz De Austri, *Dark matter and $B(s) \rightarrow \mu^+ \mu^-$ $SO(10)$ soft susy breaking*, *J. High Energy Phys.* **037** (2003) 0304 [hep-ph/0304101]; *Dark matter and $B(s) \rightarrow \mu^+ \mu^-$ $SO(10)$ soft susy breaking II*, *J. High Energy Phys.* **029** (2005) 0509 [hep-ph/0507233].
- [5] See amongst others,;
V. Berezinsky, A. Bottino, J. R. Ellis, N. Fornengo, G. Mignola and S. Scopel, *Neutralino dark matter in supersymmetric models with non-universal scalar mass terms*, *Astropart. Phys.* **5** (1996) 1 [hep-ph/9508249];
P. Nath and R. L. Arnowitt, *Non-universal soft SUSY breaking and dark matter*, *Phys. Rev. D* **56** (1997) 2820 [hep-ph/9701301];

- M. Drees, M. M. Nojiri, D. P. Roy and Y. Yamada, *Light Higgsino dark matter*, Phys. Rev. D **56** (1997) 276 [Erratum-ibid. D **64** (2001) 039901] [hep-ph/9701219].
- [6] H. Baer, A. Mustafayev, S. Profumo, A. Belyaev and X. Tata, *Neutralino cold dark matter in a one parameter extension of the minimal supergravity model*, Phys. Rev. D **71** (2005) 095008 [hep-ph/0412059].
- [7] H. Baer, A. Mustafayev, S. Profumo, A. Belyaev and X. Tata, *Direct, indirect and collider detection of neutralino dark matter in SUSY models with non-universal Higgs masses*, J. High Energy Phys. **0507** (2005) 065 [hep-ph/0504001].
- [8] J. R. Ellis, K. A. Olive and Y. Santoso, *The MSSM Parameter Space with Non-Universal Higgs Masses*, Phys. Lett. B **539** (2002) 107 [hep-ph/0204192].
- [9] J. R. Ellis, T. Falk, K. A. Olive and Y. Santoso, *Exploration of the MSSM with Non-Universal Higgs Masses*, Nucl. Phys. B **652** (2003) 259 [hep-ph/0210205].
- [10] J. R. Ellis, S. F. King and J. P. Roberts, *The Fine-Tuning Price of Neutralino Dark Matter in Models with Non-Universal Higgs Masses*, J. High Energy Phys. **0804** (2008) 099 [hep-ph/0711.2741].
- [11] H. Baer, A. Mustafayev, E. K. Park and X. Tata, *Collider signals and neutralino dark matter detection in relic-density-consistent models without universality*, J. High Energy Phys. **0805** (2008) 058 [hep-ph/0802.3384].
- [12] J. R. Ellis, T. Falk, G. Ganis, K. A. Olive and M. Schmitt, *Charginos and Neutralinos in the Light of Radiative Corrections: Sea ling the Fate of Higgsino Dark Matter*, Phys. Rev. D **58** (1998) 095002 [hep-ph/9801445];
J. R. Ellis, T. Falk, G. Ganis and K. A. Olive, *Supersymmetric Dark Matter in the Light of LEP and the Tevatron Collider*, Phys. Rev. D **62** (2000) 075010 [hep-ph/0004169].
- [13] See: <http://www.superbayes.org/>
- [14] B. C. Allanach and C. G. Lester, *Multi-dimensional MSUGRA likelihood maps*, Phys. Rev. D **73** (2006) 015013 [hep-ph/0507283];
B. C. Allanach, *Naturalness priors and fits to the constrained minimal supersymmetric standard model*, Phys. Lett. B **635** (2006) 123 [hep-ph/0601089];
B. C. Allanach, C. G. Lester and A. M. Weber, *The dark side of mSUGRA*, J. High Energy Phys. **0612** (2006) 065 [hep-ph/0609295].
- [15] R. Ruiz de Austri, R. Trotta and L. Roszkowski, *A Markov Chain Monte Carlo analysis of the CMSSM*, J. High Energy Phys. **0605** (2006) 002 [hep-ph/0602028]; see also R. Trotta, R. Ruiz de Austri and L. Roszkowski, *Prospects for direct dark matter detection in the Constrained MSSM*, [astro-ph/0609126].
- [16] L. Roszkowski, R. Ruiz de Austri and R. Trotta, *On the detectability of the CMSSM light Higgs boson at the Tevatron*, J. High Energy Phys. **0704** (2007) 084 [hep-ph/0611173].
- [17] F. Feroz, B. C. Allanach, M. Hobson, S. S. AbdusSalam, R. Trotta and A. M. Weber, *Bayesian Selection of sign(μ) within mSUGRA in Global Fits Including WMAP5 Results*, J. High Energy Phys. **10** (2008) 064
- [18] L. Roszkowski, R. Ruiz de Austri and R. Trotta, *Implications for the Constrained MSSM from a new prediction for b to s gamma*, J. High Energy Phys. **0707** (2007) 075 [hep-ph/0705.2012].

- [19] R. Trotta, F. Feroz, M. P. Hobson, L. Roszkowski and R. Ruiz de Austri, *The impact of priors and observables on parameter inferences in the Constrained MSSM*, *J. High Energy Phys.* **0812** (2008) 024 [hep-ph/0809.3792].
- [20] B. C. Allanach, *SOFTSUSY: a C++ program for calculating supersymmetric spectra*, *Comput. Phys. Commun.* **143** (2002) 305 [hep-ph/0104145].
- [21] P. Gondolo, J. Edsjo, P. Ullio, L. Bergstrom, M. Schelke and E. A. Baltz, *DARKSUSY: computing supersymmetric dark matter properties numerically*, *JCAP* **0407** (2004) 008 [astro-ph/0406204]; <http://www.physto.se/edsjo/darksusy/>.
- [22] F. Feroz and M. P. Hobson *Multimodal nested sampling: an efficient and robust alternative to MCMC methods for astronomical data analysis*, *Mon. Not. Roy. Astron. Soc.* **384** 449 (2008); F. Feroz, M. P. Hobson and M. Bridges, *MultiNest: an efficient and robust Bayesian inference tool for cosmology and particle physics* (2008), arXiv:0809.3437.
- [23] Tevatron Electroweak Working Group (for the CDF and D0 Collaborations), *A Combination of CDF and D0 Results on the Mass of the Top Quark*, hep-ex/0703034.
- [24] W.-M. Yao et al. [Particle Data Group], *J. Phys.* **G33** (2006) 1.
- [25] See <http://lepewwg.web.cern.ch/LEPEWWG>.
- [26] K. Hagiwara, A. D. Martin, D. Nomura and T. Teubner, *Improved predictions for $g-2$ of the muon and $\alpha_{\text{QED}}(M_Z^2)$* , *Phys. Lett. B* **649** (2007) 173 [hep-ph/0611102].
- [27] Heavy Flavor Averaging Group (HFAG) (E. Barberio et al.), *Averages of b -hadron properties at the end of 2005*, hep-ex/0603003; for a very recent update see Heavy Flavor Averaging Group (HFAG) (E. Barberio et al.), *Averages of b -hadron properties at the end of 2006*, arXiv:0704.3575.
- [28] The CDF Collaboration, *Measurement of the $B_s - \bar{B}_s$ oscillation frequency*, *Phys. Rev. Lett.* **97** (2006) 062003 [hep-ex/0606027] and *Observation of $B_s - \bar{B}_s$ oscillations*, *Phys. Rev. Lett.* **97** (2006) 242003 [hep-ex/0609040].
- [29] E. Komatsu et al. [WMAP Collaboration], *Five-Year Wilkinson Microwave Anisotropy Probe (WMAP) Observations: Cosmological Interpretation*, *Astrophys. J. Suppl.* **180** (2009) 330 [astro-ph/0803.0547].
- [30] T. Aaltonen et al. [CDF Collaboration], *Search for $B_s \rightarrow \mu^+ \mu^-$ and $B_d \rightarrow \mu^+ \mu^-$ Decays with 2fb^{-1} of $p\bar{p}$ Collisions*, *Phys. Rev. Lett.* **100** (2008) 101802 [hep-ex/0712.1708].
- [31] The LEP Higgs Working Group, <http://lep Higgs.web.cern.ch/LEPHIGGS>; G. Abbiendi et al. [the ALEPH Collaboration, the DELPHI Collaboration, the L3 Collaboration and the OPAL Collaboration, The LEP Working Group for Higgs Boson Searches], *Search for the standard model Higgs boson at LEP*, *Phys. Lett. B* **565** (2003) 61 [hep-ex/0306033].
- [32] K. L. Chan, U. Chattopadhyay and P. Nath, *Naturalness, Weak Scale Supersymmetry and the Prospect for the Observation of Supersymmetry at the Tevatron and at the LHC*, *Phys. Rev. D* **58** (1998) 096004 [hep-ph/9710473]; J. L. Feng, K. T. Matchev and T. Moroi, *Multi - TeV scalars are natural in minimal supergravity*, *Phys. Rev. Lett.* **84** (2000) 2322 [hep-ph/9908309]; *Focus points and naturalness in supersymmetry*, *Phys. Rev. D* **61** (2000) 075005 [hep-ph/9909334]; J. L. Feng, K. T. Matchev and F. Wilczek, *Neutralino dark matter in focus point supersymmetry*, *Phys. Lett. B* **B482** (2000) 388 [hep-ph/0004043].

- [33] M. Olechowski and S. Pokorski, *Electroweak symmetry breaking with nonuniversal scalar soft terms and large tan beta solutions*, Phys. Lett. B **344** (1995) 201 [hep-ph/9407404].
- [34] G. D. Martinez, J. S. Bullock, M. Kaplinghat, L. E. Strigari and R. Trotta, *Indirect Dark Matter Detection from Dwarf Satellites: Joint Expectations from Astrophysics and Supersymmetry* [arXiv:0902.4715]
- [35] See, e.g., G. Jungman, M. Kamionkowski and K. Griest, *Supersymmetric dark matter*, Phys. Rept. **267** (1996) 195;
C. Muñoz, *Dark Matter Detection in the Light of Recent Experimental Results*, Int. J. Mod. Phys. A **19** (2004) 3093 [hep-ph/0309346].
- [36] M. Drees and M. Nojiri, *Neutralino - nucleon scattering revisited*, Phys. Rev. D **48** (1993) 3483 (hep-ph/9307208). Phys. Rev. D **48**, 3483 (1993), hep-ph/9307208.
- [37] J. Ellis, A. Ferstl, K. A. Olive, *Reevaluation of the elastic scattering of supersymmetric dark matter*, Phys. Lett. B **481** (2000) 304 [hep-ph/0001005].
- [38] Y. G. Kim, T. Nihei, L. Roszkowski and R. Ruiz de Austri, *Upper and lower limits on neutralino WIMP mass and spin-independent scattering cross section, and impact of new $(g-2)(\mu)$ measurement*, J. High Energy Phys. **0212** (2002) 0342002 [hep-ph/0208069].
- [39] L. Roszkowski, R. R. de Austri, J. Silk and R. Trotta, *On prospects for dark matter indirect detection in the Constrained M SSM*, Phys. Lett. B **671**, 10 (2009) [astro-ph/0707.0622].
- [40] Y. Mambrini and C. Munoz, *Gamma-ray detection from neutralino annihilation in non-universal SU GRA scenarios*, Astropart. Phys. **24** (2005) 208 [hep-ph/0407158].
- [41] The CDMS Collaboration, *Limits on spin-independent WIMP-nucleon interactions from the two-tower run of the Cryogenic Dark Matter Search*, Phys. Rev. Lett. **96** (2006) 011302 [astro-ph/0509259].
- [42] V. Sanglard et al.[EDELWEISS Collaboration], *Final results of the EDELWEISS-I dark matter search with cryogenic heat-and-ionization Ge detectors*, Phys. Rev. D **71** (2005) 122002 [astro-ph/0503265].
- [43] G. J. Alner et al.[UK Dark Matter Collaboration], *First limits on nuclear recoil events from the ZEPLIN-I galactic dark matter detector*, Astropart. Phys. **23** (2005) 444.
- [44] G. J. Alner et al., *First limits on WIMP nuclear recoil signals in ZEPLIN-II: A two phase xenon detector for dark matter detection*, Astropart. Phys. **28** (2007) 287 [astro-ph/0701858].
- [45] V. N. Lebedenko et al., *Result from the First Science Run of the ZEPLIN-III Dark Matter Search Experiment*, arXiv:0812.1150 [astro-ph].
- [46] J. Angle et al. [XENON Collaboration], *First Results from the XENON10 Dark Matter Experiment at the Gran Sasso National Laboratory* Phys. Rev. Lett. **100** (2008) 021303 [astro-ph/0706.0039].
- [47] L. Bergström, et al, *Observability of Gamma Rays from Dark Matter Neutralino Annihilations in the Milky Way Halo*, Astropart. Phys. **9** (1998) 137 [astro-ph/9712318].
- [48] J. F. Navarro, C. S. Frenk and S. D. M. White, *The structure of cold dark matter halos*, Astrophys. J. **462** (1996) 563 [astro-ph/9508025] and *A universal density profile from hierarchical clustering*, Astrophys. J. **490** (1997) 493.

- [49] A. Klypin (private communication) ??and F. Prada, A. Klypin, J. Flix, M . Martinez and E. Simonneau, *Astrophysical inputs on the SUSY dark matter annihilation detectability*, Phys. Rev. Lett. **93** (2004) 241301 [astro-ph/0401512].
- [50] See: <http://tinyurl.com/yp6g5w> (as of Dec 2007).
- [51] J. Edsjö, M. Schelke and P. Ullio, *Direct versus indirect detection in mSUGRA with self-consistent halo models*, JCAP **0409** (2004) 004 [astro-ph/0405414].
- [52] E. A. Baltz and J. Edsjö, *Positron Propagation and Fluxes from Neutralino Annihilation in the Halo*, Phys. Rev. D **59** (1999) 023511 [astro-ph/9808243].
- [53] I. V. Moskalenko and A. W. Strong, *Production and propagation of cosmic ray positrons and electrons*, Astrophys. J. **493** (1998) 694 [astro-ph/9710124]; I. V. Moskalenko, et al, *Developing the Galactic diffuse emission model for the GLAST Large Area Telescope*, arXiv:0704.1328 [astro-ph].
- [54] D. Hooper and J. Silk, *Searching for Dark Matter with Future Cosmic Positron Experiments*, Phys. Rev. D **71** (2005) 083503 [hep-ph/0409104].
- [55] J. Lavalle, J. Pochon, P. Salati and R. Taillet, *Clumpiness of Dark Matter and Positron Annihilation Signal: Computing the odds of the Galactic Lottery*, arXiv:0603796 [astro-ph].
- [56] M. A. DuVernois et al., *Cosmic ray electrons and positrons from 1-GeV to 100-GeV: Measurements with HEAT and their interpretation*, Astrophys. J. **559** (2001) 296.
- [57] O. Adriani et al., *Observation of an anomalous positron abundance in the cosmic radiation*, arXiv:0810.4995
- [58] D. Hooper, P. Blasi and P. D. Serpico, *Pulsars as the Sources of High Energy Cosmic Ray Positrons*, JCAP **0901** (2009) 025 [astro-ph/0810.1527]; S. Profumo, *Dissecting Pamela (and ATIC) with Occam's Razor: existing, well-known Pulsars naturally account for the 'anomalous' Cosmic-Ray Electron and Positron Data*, astro-ph/0812.4457.